

A comparison between magnetic shear and flare shear in a well-observed M-class flare *

Tuan-Hui Zhou^{1,2} and Hai-Sheng Ji¹

¹ Purple Mountain Observatory, Chinese Academy of Sciences, Nanjing 210008, China;
thzhou@pmo.ac.cn

² Graduate School of the Chinese Academy of Sciences, Beijing 100049, China

Received 2008 April 9; accepted 2009 January 5

Abstract We give an extensive multi-wavelength analysis of an eruptive M1.0/1N class solar flare, which occurred in the active region NOAA 10044 on 2002 July 26. Our emphasis is on the relationship between magnetic shear and flare shear. Flare shear is defined as the angle formed between the line connecting the centroids of the two ribbons of the flare and the line perpendicular to the magnetic neutral line. The magnetic shear is computed from vector magnetograms observed at Big Bear Solar Observatory (BBSO), while the flare shear is computed from Transition Region and Coronal Explorer (TRACE) 1700 Å images. By a detailed comparison, we find that: 1) The magnetic shear and the flare shear of this event are basically consistent, as judged from the directions of the transverse magnetic field and the line connecting the two ribbons' centroids. 2) During the period of the enhancement of magnetic shear, flare shear had a fast increase followed by a fluctuated decrease. 3) When the magnetic shear stopped its enhancement, the fluctuated decreasing behavior of the flare shear became very smooth. 4) Hard X-ray (HXR) spikes are well correlated with the unshearing peaks on the time profile of the rate of change of the flare shear. We give a discussion of the above phenomena.

Key words: Sun: flare — Sun: magnetic field — Sun: sunspot

1 INTRODUCTION

It is well accepted that solar flares are due to a sudden release of non-potential magnetic energy. Observationally, one of the most important parameters for evaluating non-potential magnetic energy is the magnetic shear computed from vector magnetograms (Zhang 2001). Magnetic shear is defined as the excess of the observed azimuth of the vector field over the azimuth of the potential field calculated from the observed distribution of magnetic flux (Hagyard 1984). It has been found that the magnetic shear may decrease, increase, or remain unchanged after flares occur (Wang 1992; Ambastha et al. 1993; Chen et al. 1994; Wang et al. 1994, 2004; Li et al. 2000a,b). A puzzling result is that the magnetic shear around the flaring magnetic polarity inversion line (PIL) may actually increase after flares (e.g., Ambastha et al. 1993; Chen et al. 1994; Wang et al. 1994), which seems to indicate energy buildup, rather than release. This result poses a contradiction for the requirement of releasing magnetic energy to power flares.

The magnetic shear is sometimes estimated from flare loops or their footpoints (FPs). In order to distinguish the difference, this kind of shear is defined as flare shear (Ji et al. 2007). By estimating magnetic shear in this way, several authors have reported less sheared flaring structure after flares (Masuda

* Supported by the National Natural Science Foundation of China.

et al. 2001; Asai et al. 2003; Bogachev et al. 2005; Ji et al. 2006; Zhou et al. 2008). For the tendency for unshearing, it is believed that the outer magnetic field lines are less sheared than the inner field lines (Moore et al. 2001). Using high-cadence H_{α} observation for an M-class flare at the GanYu Solar Station, Ji et al. (2006) reported that the flare shear has a steady decrease during the flare despite the rather complex moving patterns of optical, radio and hard X-ray (HXR) sources of the flare. Furthermore, for that event, the time profile for the rate of change of flare shear (unshearing rate) seems to be correlated with the flare's HXR emissions. On the time profile, there appear many fine temporal structures whose physical significance needs further investigations with high-quality data.

It can be seen from the above brief introduction that there actually exist two kinds of shears that account for the non-potentiality of the magnetic field during flares: magnetic shear and flare shear. The two kinds of shears may correlate with each other or have a physical relationship. However, this correlation/relation has never been revealed from observations.

With the above motivation, in this paper, we analyze an M1.0 flare, which occurred in active region NOAA 10044 on 2002 July 26. The flare shows a strong shearing motion along its ribbons and it is associated with the rapid emergence of highly-sheared magnetic flux. Tan & Ji (2006) reported that there was a rapid drop in electric currents associated with this flare. They proposed that the reconnection site of this flare should be near the photosphere. All of the above features provide us with a good opportunity to investigate the relationship between magnetic shear and flare shear.

2 OBSERVATIONS

We use vector magnetograms observed by the Digital Vector Magnetograph (DVMG) of BBSO to evaluate magnetic shear. At BBSO, a Ca I line at 6103 \AA is used to obtain vector magnetograms with a 1 minute cadence. The hardware and other details of DVMG have been described by Spirock et al. (2002). For the vector magnetograph, the line-of-sight magnetic sensitivity is approximately 2 G, while the transverse sensitivity is approximately 20 G. We use the algorithm developed by the BBSO group to derive the vector magnetic field components. The accurate position information of BBSO's images is determined by aligning with MDI continuum images, taking sunspots as references. The accuracy of the alignment is about $2''$. To resolve the 180° azimuth ambiguity, we use a method developed by Moon et al. (2003). The results are additionally checked by using a method developed by Metcalf (1994). We find that both methods give agreeable results for this active region (Tan et al. 2006).

We use 1700 \AA images observed by TRACE to analyze the flare ribbons' motion. One important advantage of space data is that it is free from the effects of seeing, which is crucial for studying fine temporal structures. A TRACE 1700 \AA image is dominated by UV continuum ($4 - 10 \times 10^3 \text{ K}$), resembling a visible image of the temperature minimum taken in the CN bandhead or the wings of the K line (Handy et al. 1999). On TRACE 1700 \AA images, the flare has two ribbons. We use the center-of-mass method (CoM) to determine the centroid positions of flare ribbons (Ji et al. 2004), using background-subtracted images. For comparison, we also take the 50% contour line as the threshold to compute the centroid positions of the ribbons. For this flare, there is no saturation in TRACE images. For TRACE images, sometimes there may be a small error in pointing. With the help of MDI continuum images, we use TRACE white light images taken during the flare to determine the accurate position information of TRACE 1700 \AA images. The accuracy of the alignment is about $2''$.

The Reuven Ramaty High Energy Solar Spectroscopic Imager (*RHESSI*) had good coverage of this event. *RHESSI* was designed to investigate particle acceleration and energy release in solar flares through imaging and spectroscopy of hard X-ray/gamma-ray continua emitted by energetic electrons and ions (Lin et al. 2002). The spatial resolution is as fine as ~ 2.3 arcsec and the time resolution for constructing images with sufficient counts is several seconds. We use the CLEAN (Hurford et al. 2002) reconstruction algorithm to make HXR maps. The integration time for making a CLEAN map is 20 s.

3 RESULTS

This flare is impulsive and is of Geostationary Operational Environmental Satellites (*GOES*) soft X-ray importance M1.0, lasting ~ 12 minutes. Figure 1 displays the flaring process, as observed in the H_{α} line

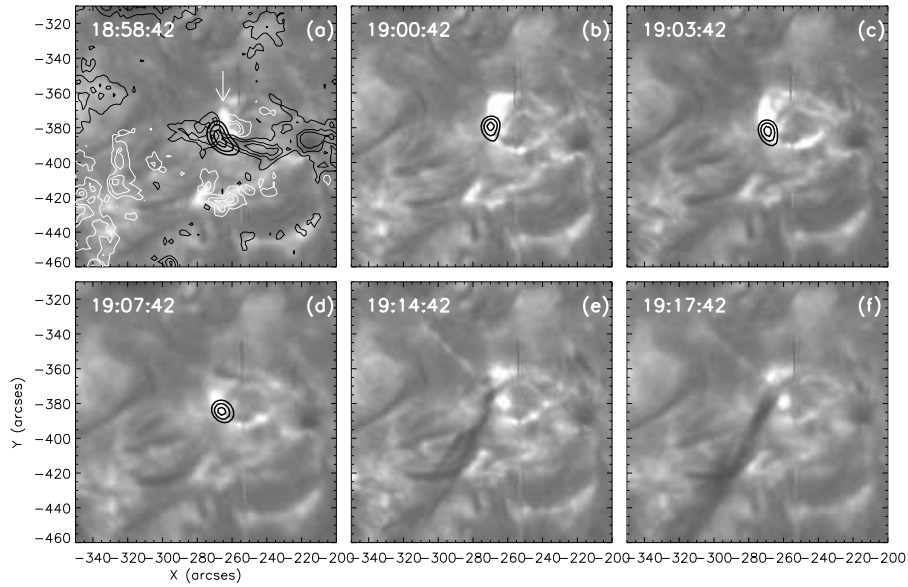


Fig. 1 Evolution of the flare in H_{α} line center images observed at BBSO. The thick black contours in panels a-d are from *RHESSI* clean maps in the energy range of 12–25 keV. The thin black and white contours in panel a represent the positive and negative longitudinal magnetic field.

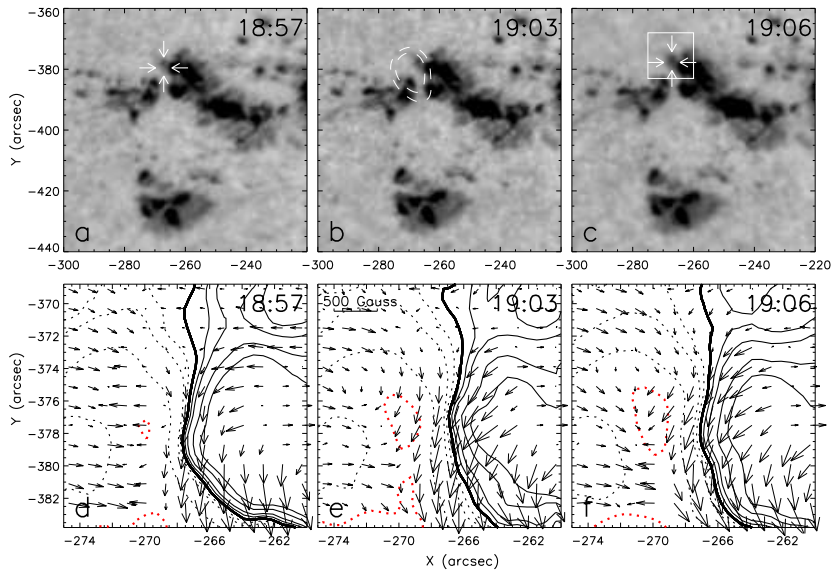


Fig. 2 a–c: Time sequence of BBSO Stokes *I* images showing the evolution of the active region. The formation of the satellite sunspot is pointed out by the arrows in panels a and c. The dashed white contours in panel b show the site of hard X-ray emission in the energy band of 12–25 keV as observed by *RHESSI*. d–f: Time sequence of BBSO vector magnetograms shows the evolution of the magnetic field corresponding to the formation of the sunspot. The solid and dotted contours (emerging) represent the positive and negative longitudinal magnetic field, respectively. The levels of the contours are ± 100 , ± 300 , ± 500 and ± 700 G, respectively.

center at BBSO. The two kernels of the flare are mingled together (Fig. 1e-f). There was a surge ~ 10 minutes after the onset of the flare (Fig. 1).

There is only one HXR source throughout the flare. The single HXR source is not co-spatial with the initial H_α brightening patch (Fig. 1a). There is an offset of over 6 arcsec between them at the very beginning of the flare. We suppose that the HXR source is above the site of the H_α emission. Thus, the single HXR source can be regarded as the kind with loop-top emission.

Figure 2a-c show three BBSO Stokes I images during the flare, from which we can see the formation of a small satellite sunspot, whose position is pointed out by arrows in panels a and c. The region selected for a detailed analysis of vector magnetograms is marked by a white rectangular box in Figure 2c.

Figure 2d-f show three corresponding vector magnetograms in the boxed region in Figure 2c. We can see that the satellite sunspot is of negative (leading) polarity. From the contours (see: red contour in Fig. 2d-f) of the negative longitudinal magnetic field, it can be seen that the emergence is very rapid. From the transverse component shown by the vectors on the magnetograms, we can see that the original leading flux and, especially, the newly-emerged flux are highly sheared.

The time profile of the normalized mean intensity within the box obtained from the Stokes I images is shown in Figure 3a. In Figure 3, a vertical dotted line marks the starting time (18:57:30 UT) of the flare, as determined from the *RHESSI* light curve in the energy band of 12–25 keV. The mean intensity around the satellite sunspot (top panel) drops rapidly after the onset of the flare, showing that the formation of the satellite sunspot is very rapid.

The negative and positive magnetic fluxes within the region have a rapid increase and rapid decrease respectively (Fig. 3b-c) (also see Tan & Ji 2006). The changes are permanent and I images clearly show the formation of the satellite sunspot. Therefore, it is unlikely that they are caused by flare-induced line profile changes (Patterson et al. 1984; Ding et al. 2002). The rapid, permanent, and imbalanced changes of the magnetic field during major solar flares have been reported and studied by many authors (Wang et al. 2002; Spirock et al. 2002; Yurchyshyn et al. 2004; Sudol et al. 2005). This flare is a much weaker event compared with those flares associated with rapid magnetic changes.

Because the flare is located near the center of the solar disk, we neglect the projection effect (Li 2002). Using the Green's function method (Chiu & Hilton 1977), we computed the potential field in this active region and got the magnetic shear values by comparing the observed transverse field with the computed potential transverse field. The value of magnetic shear has a corresponding enhancement, as shown in Figure 3d. The rapid enhancement for the magnetic fluxes and magnetic shear begins at around 18:59 UT and ends at 19:04 UT, which are marked by two dashed lines in Figure 3.

Figure 4 gives the flaring process on the 1700 Å images observed by TRACE. We can see that the flare is a small two-ribbon flare. The EUV emission of the flare comes predominantly from the two boxed regions in Figure 4b. The time profiles of the two regions' emission strongly correlate with each other and the correlation coefficient is found to be over 0.995 (Fig. 5). Furthermore, there is only one dominant kernel in ribbons a1 and a2 respectively, judged from the brightness contours of the ribbons (Fig. 4b). Therefore, the two small ribbons can be regarded as a pair of conjugate ones. We computed the centroids of the two ribbons in the boxed regions in Figure 4b with the center-of-mass method.

There is a strong shearing motion parallel to the neutral line in addition to a separation motion. With respect to the neutral line, the distance between the centroids of the two ribbons is decomposed into two components, which are perpendicular and parallel to the neutral line respectively. From the perpendicular component, we can get the usual separation motion. Thus, we will use separation motion to refer to the perpendicular motion. For the parallel component, we will use shearing motion and shearing distance. The flare shear is the angle formed by a line connecting the centroids of two conjugate flare ribbons and the line perpendicular to a simplified neutral line separating the two ribbons (Fig. 4c). As we will see, the value of flare shear is mainly affected by the shearing motion.

Firstly, we use background-subtracted images to compute the centroid positions of flare ribbons. The results are given in Figure 6. The time profiles of the shearing distance (parallel distance), the flare shear and the perpendicular distance are shown in Figure 6a-c. The lengths of the error bars are equal to the standard deviation computed from pre-flare phase images using the same boxes. Both the shearing distance and the flare shear share a similar time profile, showing a dominant shearing motion in this

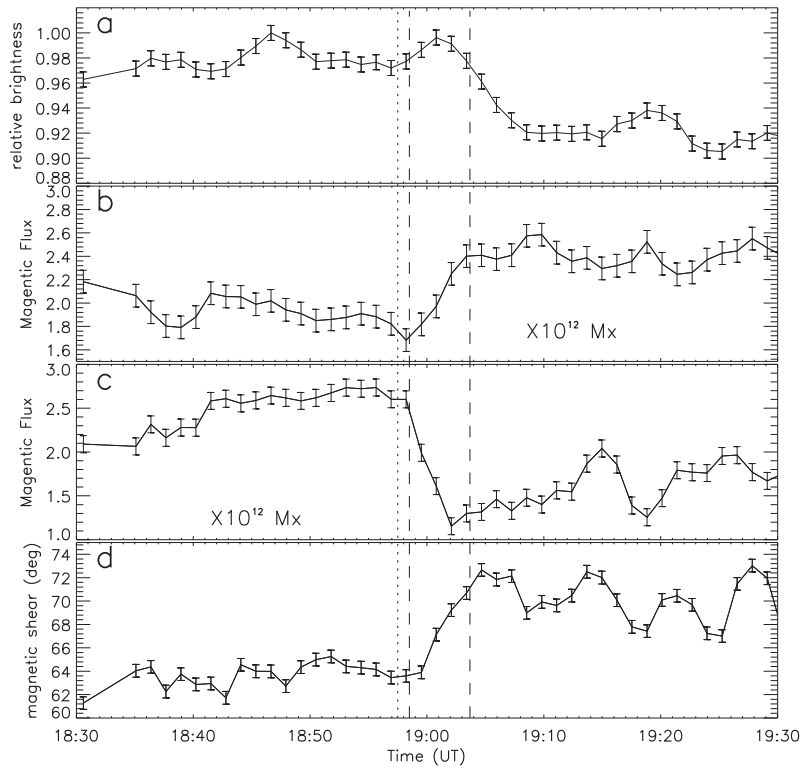


Fig. 3 Time profiles for a number of quantities. a: Normalized mean intensity around the satellite sunspot obtained from BBSO Stokes I images, which is in the boxed region in Fig. 2c. b-c: Negative and positive magnetic fluxes, which are obtained within the white box in Fig. 2c. d: Magnetic shear. The dotted line indicates the starting time of the flare, while the two dashed lines indicate the period of rapid emergence of the sheared magnetic flux.

flare. Also, the value of the flare shear is consistent with the direction of the transverse magnetic field (Fig. 2d-f). When magnetic shear and magnetic flux begin to have a rapid change at about 18:59 UT, flare ribbons have a simultaneous impulsive shearing motion, which enhances shearing distance and flare shear considerably. The enhanced shearing motion is mainly caused by ribbons a1, which move to the site of flux emergence. The moving direction is indicated by an arrow in Figure 4a. This phenomenon shows that, during the initial phase of the flare, flare shear is rapidly built up in accordance with the enhancement of magnetic shear. It is worth mentioning that, before 18:58:40 UT, the flare shear decreases slightly (Fig. 6a-b), showing the signature of relaxation of a pre-existing sheared magnetic field.

After the rapid increase, the flare shear decreases, which can be seen from the time profiles of the shearing distance as well as the flare shear (Fig. 6a-b). This clearly indicates the relaxation of the sheared magnetic field. Furthermore, the decrease of flare shear is highly fluctuated. The fluctuation occurs during the period of the enhancement of magnetic shear ($\sim 18:59 - 19:04$ UT). During this period, both build-up and relaxation of magnetic shear may co-exist, giving rise to the second larger HXR peak (Fig. 6e). After $\sim 19:04$, when the magnetic shear stops increasing, there appears a very smooth decrease of the flare shear, showing a pure relaxation of the sheared magnetic field.

As mentioned above, there appeared a single HXR source observed by *RHESSI*. The HXR energy range is up to ~ 50 keV. The red contours overlaid in Figure 4 show the position of the HXR source in the energy range of 12–25 keV. From its relative position to the flare ribbons (Fig. 4a), we can classify the

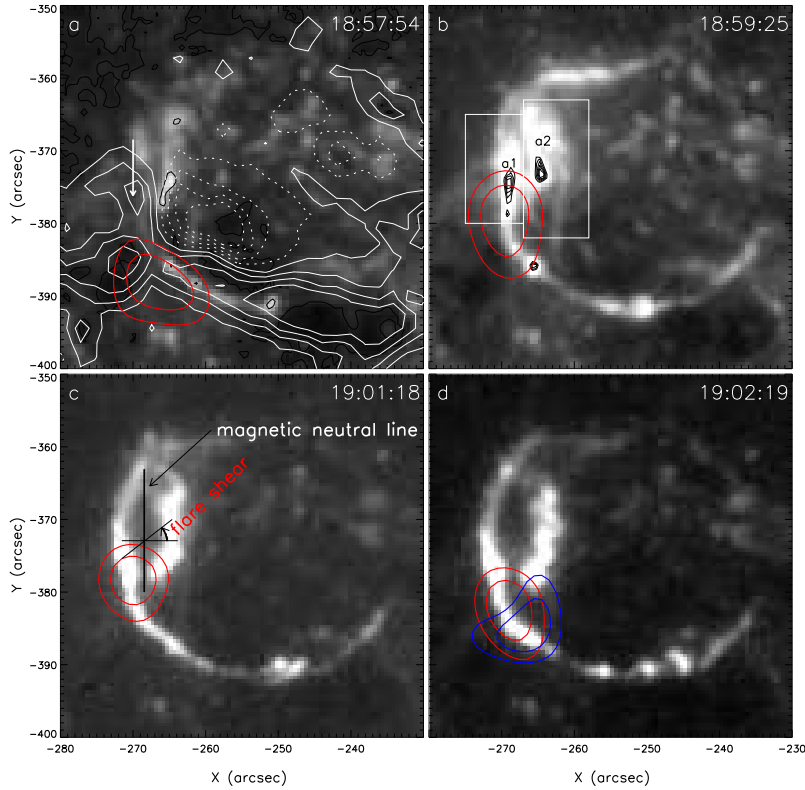


Fig. 4 TRACE 1700 Å images for the flare. In panel a, the solid and dotted white contours represent the positive and negative longitudinal magnetic field, whose levels are ± 100 , ± 300 , ± 500 , and ± 700 Gauss. The arrow in panel a indicates the emerging flux region and the moving direction of ribbon a1. Red contours are HXR emission in the energy range 12–25 keV, while blue contours are HXR emission in the energy range 25–50 keV. Black contours in the two ribbons (panel b) are 50%, 60%, 70%, 80% and 90% of the maximum value of the two ribbons.

HXR source as a loop-top source. Only during the period around 19:02 are we able to make a CLEAN map with an unambiguous source in the energy range of 25–50 keV. The source of HXR emission at 25–50 keV is spatially within the emission range at the lower energy range (blue contours in Fig. 4d). The HXR looptop source at the higher energy range is explained by Veronig & Brown (2004) by employing a coronal thick-target model. For this event, it is possible since there is a C-class pre-flare, the coronal loops should be dense with evaporated plasma.

From Figure 4, we can see that the HXR source has an apparent motion. The motion with respect to the ribbons' separation motion would be interesting, as mentioned by Ji et al. (2004, 2006). Using a tool provided by *RHESSI* software (Image Flux in *RHESSI* GUI), we measured the centroid position of the loop-top source. However, it is difficult to determine the height of the loop-top source. We measured the distance from the centroid of the loop-top source to the line that connects the centroids of two initial TRACE flaring ribbons, taking it as a projected height. The time profile for the 'height' of the loop-top source is given in Figure 6d. From the time profile of the perpendicular distance (Fig. 6c), we can find that there appears an inward (converging) motion before the ribbons move apart. The curve of the perpendicular distance is well correlated with the 'height' curve of the HXR loop-top source. Based on previous results made by *RHESSI* and other instruments (Sui et al. 2003, 2004; Ji et al. 2004,

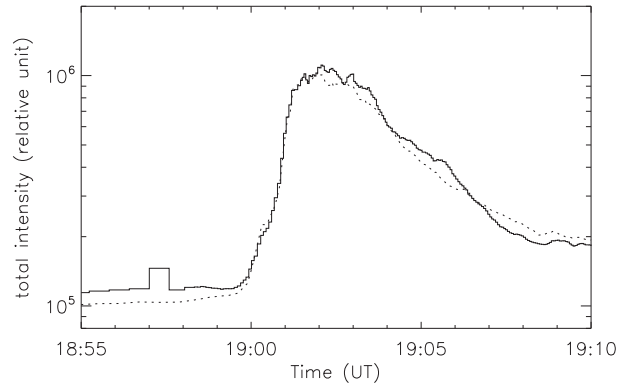


Fig. 5 Time profiles of the EUV emissions of two boxed regions of the ribbons. The correlation coefficient is over 0.995. The solid and dotted profiles represent ribbon1 and ribbon2, respectively.

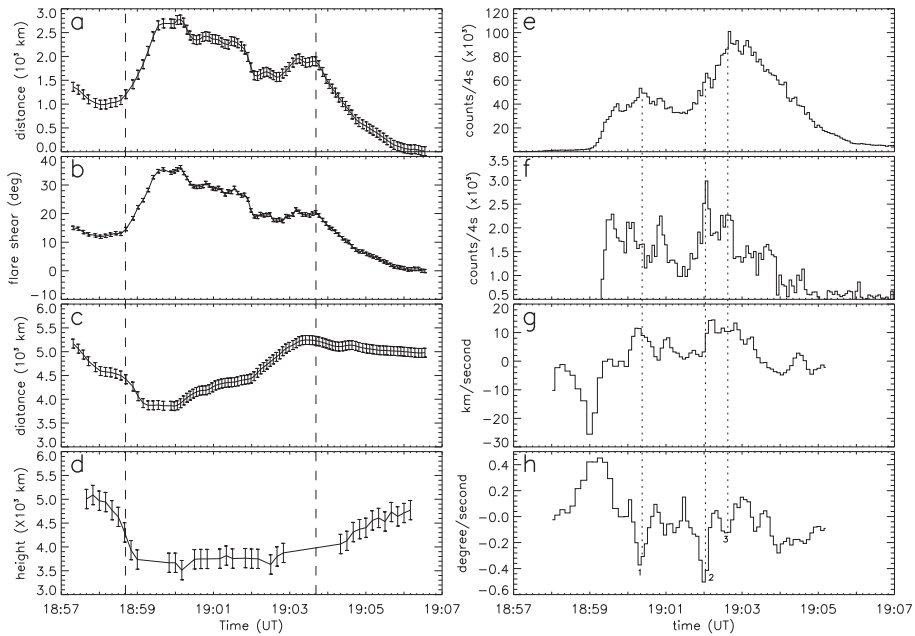


Fig. 6 Time profiles for a number of quantities. a: Parallel distance (shearing distance) between the UV ribbons. b: Flare shear. c: The perpendicular distance. d: The ‘height’ of the HXR source at 12–25 keV. e-f: The HXR emissions in the energy range of 12–25 keV and 25–50 keV. g: Perpendicular speed. h: The rate of change of the flare shear. As in Fig. 3, two dashed lines indicate the period of the rapid emergence of the sheared magnetic flux.

2006; Veronig et al. 2006; Li et al. 2005, 2006), the HXR source may have a downward motion and a subsequent upward motion.

From time profiles of the perpendicular distance and the flare shear, we derive separation speed and the rate of the change of the flare shear. The results are plotted in Figure 6g-h. For comparison, we plot the light curves of HXR in the energy bands of 12–25 keV and 25–50 keV in Figure 6e-f. Firstly, it can

be seen that the separation speed (Fig. 6g) is somehow correlated with the HXR emissions, especially in the energy range of 12–25 keV. This confirms earlier results made by a number of authors (e.g., Wang et al. 2003). Furthermore, there also appear a number of peaks on the time profile of the rate of the change of flare shear (Fig. 6h). There are three peaks, which are well above the noise level and labeled as 1–3. Both peak 2 and peak 3 can be found to be temporally correlated with the HXR peaks at 12–25 keV as well as at 25–50 keV. Peak 1 is only correlated with a HXR peak at 12–25 keV.

For comparison, we computed the centroid positions of the EUV ribbons using the 50% contour as a threshold. This actually gives the positions of flare kernels, which reflects the process of a higher energy range. The results are shown in Figure 7. From the time profile for the rate of change of flare shear (Fig. 7c), we can see that: 1) peak 2 still exists while peak 1 becomes weakened and peak 3 vanished; 2) there appear two additional peaks α and β , which are seen to be correlated with two HXR peaks at 25–50 keV.

The correlation further shows that the magnetic reconnection in the sheared magnetic field plays an important role in powering the flare, even in powering a high energy process. Here, it is worth noting that the highest peak on the unshearing curve, peak 2, is 2–3 s ahead of the corresponding HXR peak. A detailed comparison with high-cadence observations will be helpful for understanding the unshearing motion in powering high energy processes in flares. Generally speaking, we can conclude that the magnetic reconnection of this flare occurs in a highly-sheared magnetic field created by the rapid flux emergence.

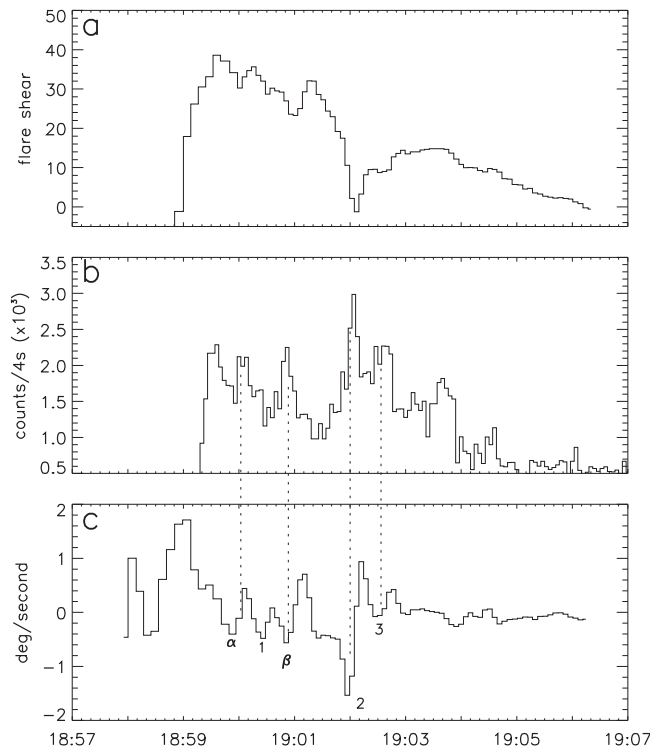


Fig. 7 a: Time profiles for the flare shear. b: The HXR emission in the energy range of 25–50 keV. c: The rate of change of the flare shear. The flare shear in this figure was computed using a 50% contour as a threshold.

4 DISCUSSION AND CONCLUSIONS

Using multiwavelength analysis, we analyzed an M1.0 class two-ribbon flare, which occurred in active region NOAA 10044 on July 26, 2002, with an emphasis on the relationship between magnetic shear and flare shear. The magnetic shear is computed from vector magnetograms observed at BBSO, while the flare shear is computed from TRACE 1700 Å images. The relationship between magnetic shear and flare shear can be summarized as follows:

- 1) We found that the magnetic shear and the flare shear of this event are basically consistent. The direction of the line connecting the centroids of the two ribbons is consistent with the overall direction of the transverse magnetic field. Such a consistency is due to the fact that the spatial scale of the flare is small and the flare loops are adjacent to the photosphere. Therefore, the direction of the flare loops is consistent with the overall direction of the transverse magnetic field.
- 2) During the period of the enhancement of the magnetic shear, which took about three minutes, the flare shear had a fast increase (less than one minute) followed by a fluctuated decrease. Unlike the behavior of the flare shear, whose enhancement was finally reduced, the increase of the magnetic shear seems to be permanent.
- 3) When the magnetic shear stopped its enhancement, the fluctuated decreasing behavior became very smooth.
- 4) We find that the HXR spikes are well correlated with the unshearing peaks on the time profile of the rate of the change of the flare shear.

According to formula (14) given by Ji et al. (2007), we can see that the tangent of the flare shear is proportional to two factors: the force free parameter α and the height scale factor γ^{-1} of the magnetic field. The emergence of the sheared magnetic field will enhance the α value and, thus, the value of flare shear. The release of magnetic energy in the corona will reduce the value of the height scale factor γ^{-1} . This shows that flare shear can reflect the dynamic process of the release of magnetic energy in the corona. Magnetic shear only reflects the driving process from the photosphere, whose time scale is usually much longer. According to the formula (12) given by Ji et al. (2007), the flare shear is directly related to free magnetic energy. So, the unshearing peaks are the signature of rapid release of free magnetic energy.

The time profile of the perpendicular distance shows that, during the initial phase of the flare, there is a significant inward (converging) motion for the flare ribbons before they move apart. Meanwhile, the HXR looptop source has a well correlated downward and subsequent upward motion. Ji et al. (2007) reported that the flare shear was decreasing through the contraction phase to the expansion phase. However, in this event, the flare shear increased first and then decreased. Based on the above discussion and the behavior of magnetic shear, we can say that the increase of flare shear in the initial phase is caused by the increase of magnetic shear.

All of the above shows that flare shear can be an important parameter for studying flare dynamics, especially when it is combined with magnetic shear. Nevertheless, we need to analyze more events, especially those two ribbon flares with small spatial scales, to study the relationship between magnetic shear and flare shear. We will carry out similar studies in the near future. Further investigations will be of a statistical nature, including the estimate of free magnetic energy for different flares using formula (12) given by Ji et al. (2007).

Acknowledgements Both authors would like to thank the anonymous referee for his/her suggestions for improving the paper. We are grateful to the BBSO observing staff for their support. The authors would like to thank TRACE and SOHO/MDI for providing data. SOHO is a project of international cooperation between ESA and NASA. We are especially grateful to the *RHESSI* team for providing *RHESSI* data and software. The work is supported by the NSFC Nos. 10473024, 10333030 and 973 project with No. 2006CB806302.

References

- Ambastha, A., Hagyard, M. J., & West, E. A. 1993, *Sol. Phys.*, 148, 277
- Asai, A., Ishii, T. T., Kurokawa, H., et al. 2003, *ApJ*, 586, 624
- Bogachev, S. A., Somov, B. V., Kosugi, T., et al. 2005, *ApJ*, 630, 561
- Chen, J., Wang, H., Zirin, H., et al. 1994, *Sol. Phys.*, 154, 261
- Chiu, Y. T. & Hilton, H. H. 1977, *ApJ*, 212, 873
- Ding, M. D., Qiu, J., & Wang, H. 2002, *ApJ*, 576, L83
- Hagyard, M. J., Smith, J. B., Teuber, D., et al. 1984, *Sol. Phys.*, 91, 115
- Handy, B. N., et al. 1999, *Sol. Phys.*, 187, 229
- Hurford, G., Schmahl, E., et al. 2002, *Sol. Phys.*, 210, 61
- Ji, H., Wang, H., Goode, P. R., et al. 2004, *ApJ*, 607, L55
- Ji, H., Huang, G., Wang, H., et al. & Song, M. 2006, *ApJ*, 636, L173
- Ji, H., Huang, G., Wang, H. 2007, *ApJ*, 660, 893
- Li, H. 2002, *ChJAA (Chin. J. Astron. Astrophys.)*, 2, 174
- Li, H., Sakurai, T., Ichimoto, K., & UeNo, S. 2000a, *PASJ*, 52, 483
- Li, H., Sakurai, T., Ichimoto, K., & UeNo, S. 2000b, *PASJ*, 52, 465
- Li, Y. P. & Gan, W. Q. 2005, *ApJ*, 629, L137
- Li, Y. P. & Gan, W. Q. 2006, *ApJ*, 644, L97
- Lin, R. P., Dennis, B. R., & Hurford, G. J., et al. 2002, *Sol. Phys.*, 210, 3
- Masuda, S., Kosugi, T., & Hudson, H. S. 2001, *Sol. Phys.*, 204, 55
- Metcalf, T. 1994, *Sol. Phys.*, 155, 235
- Moon, Y.-J., Wang, H., Spirock, T. J., et al. 2003, *Sol. Phys.*, 217, 79
- Moore, L., Sterling, A., Hudson, S., 2001, *ApJ*, 552, 833
- Patterson, A. 1984, *ApJ*, 280, 884
- Spirock, T. J., Yurchyshyn, V., & Wang, H. 2002, *ApJ*, 572, 1072
- Sudol, J. J., & Harvey, J. W., 2005, *ApJ*, 635, 647
- Sui, L., & Holman, D. 2003, *ApJ*, 596, L251
- Sui, L., Holman, G. D. & Dennis, B. R. 2004, *ApJ*, 612, 546
- Tan, B., & Ji, H. 2006, *Sol. Phys.*, 239, 137
- Veronig, A. M., Brown, J. C., 2004, *ApJ*, 603, L117
- Veronig, A. M., Karlicky, M., Vrsnak, B., et al. 2006, *A&A*, 446, 675
- Wang, H. 1992, *Sol. Phys.*, 140, 85
- Wang, H., Ewell, M. W. Jr., Zirin, H., et al. 1994, *ApJ*, 424, 436
- Wang, H., Spirock, T., Qiu, J., et al. 2002, *ApJ*, 576, 497
- Wang, H., Qiu, J., Jing, J., & Zhang, H. 2003, *ApJ*, 593, 564
- Wang, H., Qiu, J., Jing, J., et al. 2004, *ApJ*, 605, 931
- Wang, H. 2006, *ApJ*, 649, 490
- Yurchyshyn, V., Wang, H., Abramenko, V., et al. 2004, *ApJ*, 605, 546
- Zhang, H. 2001, *ApJ*, 557, L71
- Zhou, T., Ji, H. 2008, *Advances in Space Research*, 41, 1195